applied sciences

MDPI

Article

Mixed-Layer Illite-Smectite Illitization under Supercritical CO_2 Conditions

Domingo Martín [1,*], Patricia Aparicio [1], Susana García [2] and María Mercedes Maroto-Valer [2]

[1] Departamento Cristalografía, Mineralogía y Química Agrícola—Universidad de Sevilla, 41012 Seville, Spain
[2] Research Centre for Carbon Solutions (RCCS), School of Engineering and Physical Sciences, Heriot-Watt University, Edinburgh EH14 4AS, UK
* Correspondence: dmartin5@us.es; Tel.: +34-9545-56320

Abstract: The long-term safe storage of CO_2 in geological reservoirs requires the understanding of the impact of CO_2 on clay-rich sealing cap rocks. The reactivity of the mixed layer of illite-smectite was investigated to determine the reaction pathways under conditions of supercritical CO_2 ($scCO_2$) conditions in the context of geological CO_2 storage. A common clay (blue marl from the Guadalquivir Tertiary basin, southern Spain) was tested under brine $scCO_2$ conditions (100 bar and 35 °C) for 120 and 240 h. The clay sample (blue marl) contains calcite, quartz, illite, smectite, and the corresponding mixed-layer and kaolinite. X-ray diffraction (XRD), Brunauer–Emmett–Teller (BET), and inductively coupled plasma optical emission spectroscopy (ICP-OES) analyses were performed. The illitization of mixed-layer illite-smectite was observed by XRD and confirmed by a variation in the content of different elements (K, Mg, Na, Ca, and Fe) of the transformation, as well as an increase in the specific surface (SSA) of the clay (36.1 to 38.1 m^2/g by N_2, 14.5 to 15.4 m^2/g by CO_2 adsorption). Furthermore, these reactions lead to mineral dissolution and secondary mineral formation along the CO_2–water–clay intercalations of the source rock were responsible for a change in porosity (7.8 to 7.0 nm pore size). The implications of illitisation, mineral destruction, and precipitation processes on CO_2 storage and clay layer integrity should be explored before deciding on a geological storage location.

Keywords: carbon geological storage; sealing cap rock; common clay; mixed-layer illite-smectite; illitization; marls

Citation: Martín, D.; Aparicio, P.; García, S.; Maroto-Valer, M.M. Mixed-Layer Illite-Smectite Illitization under Supercritical CO_2 Conditions. *Appl. Sci.* **2022**, *12*, 11477. https://doi.org/10.3390/app122211477

Academic Editors: Johannes Schwank and Nikolaos Koukouzas

Received: 9 October 2022
Accepted: 9 November 2022
Published: 11 November 2022

1. Introduction

The extensive use of fossil fuels is a major source of greenhouse gas (GHG) emissions, especially carbon dioxide, and is a major contributor to global warming. The main current efforts are devoted to the development of sustainable technologies to reduce CO_2 emissions, even to achieve net zero or negative emissions [1]. The United Nations Paris Climate Agreements, signed in 2016, established a limit for global warming below 2 °C, ideally 1.5 °C above preindustrial levels [2–4]. The concept of zero carbon emissions implies that for every amount of CO_2 produced by human activity, the same amount must be removed from the atmosphere, either by preventing its direct emission or compensating for the existing concentration of CO_2 in the atmosphere. In this way, the concentration of CO_2 concentration in the atmosphere and the global average temperature would be prevented from increasing [5].

Carbon capture and storage (CCS), together with carbon capture and utilization (CCU) or a combination of both (carbon capture, utilization and storage, CCUS), are technologies that have a role to play in achieving the objectives outlined above [6]. Geological CO_2 Storage (GCS) underground is one of the ways to contain anthropogenic emissions included in CCS strategies. In GCS, supercritical CO_2 is injected and stored long-term [7,8].

Before injection, for geological storage to be successful, the storage location must meet three fundamentals: (1) high storage capacity, (2) feasibility for injection, and (3) safe storage over time. Safety is a critical condition because CO_2 leakage poses significant risks

to other resources such as drinking groundwater, vegetation, and animal life, as well as to human health, despite the return of CO_2 to the atmosphere [8–15]. During the CO_2 storage process, the CO_2 and host and sealing rock interactions should be considered. The main concern in terms of CO_2-rock interactions in this storage stage is a possible decrease in permeability around the well that could affect injection rates and generate overpressures in the reservoir [16]. Large gas transfers characterize the injection phase through the pore space under high pressures and potentially large temperature gradients. Large temperature gradients can play a role in the interactions between CO_2 and rock, but the presence of moisture must also be considered. In terms of geochemical interactions, some reactions must be considered. These reactions include carbonate minerals, as well as sulphate and evaporite minerals, as their reaction kinetics are intense and equilibrium is reached instantaneously [17,18].

CO_2–rock interactions during storage can be studied by field and laboratory experiments, including computational simulations. Recently, these simulations have been of great interest to the scientific research community. At the beginning of this millennium, Johnson and his collaborators [19] developed the first comprehensive approach to validate the simulation of the interactions that result from the injection of CO_2 injection into the host rock.

In long-term interactions, the brine produced by the dissolution of supercritical CO_2 in water plays a significant role. Both CO_2 dissolved in brine and its acidification cause chemical interactions with the host rock, and in some proportion in the sealing rock. The importance of studying long-term interactions is to predict the reservoir's ability to permanently trap CO_2 as a mineral phase (known as mineral trapping or mineral carbonation). In the case of cover rock, the purpose of the analysis is to evaluate changes in the permeability of the induced porosity, especially at the bottom. These geochemical interactions, which affect aluminum-silicate minerals, such as Ca-/Mg-rich silicates, feldspars, or clay minerals, are characterized by prolonged reaction rates, which in some cases require thousands of years to reach equilibrium [20,21].

Nevertheless, more viable cap rocks are rocks in which carbonation is negligible because the impact on porosity and permeability is of significant interest to avoid risks that weaken the sealing integrity. Several authors [22–26] concluded that the geochemical impact and consequent porosity changes induced by CO_2 through the diffusion of cap rocks are minor and limited to the host and cap rock interface. Other authors, such as Jia and Xina [27], predicted petrophysical aspects using realistic data in pore models such as shale formations.

Knowledge of the behavior of sealing rock, and in particular clayey rock with CO_2, becomes necessary to prevent risks of leakage from stored gas. These leakages can affect the geochemistry of the environment near the storage site, potable water, and prevent CO_2 from escaping uncontrollably into the atmosphere [28,29].

This laboratory study aimed to determine the interactions between a type of clay-based sealing rock and CO_2 under supercritical conditions. Economic reasons include saving costs of transporting CO_2 from the capture plants to the storage site [8], enhanced oil recovery methodologies (EOR), and methodologies with carbon dioxide [30]. Extensive supercritical CO_2 storage projects are being developed [31,32]. Changes in the mineralogy of the sealing rock that may be susceptible to leakage of the confined gas were analyzed to ensure the efficiency and stability of geological storage.

2. Materials and Methods

2.1. Blue Marl as Sealing Rock

A common clay, blue marl, from the Guadalquivir Tertiary basin (S. Spain) was used as a sealing rock at a low CO_2 pressure and room temperature in previous studies [33,34]. In these studies, blue marl was used as a sealing rock in a secondary role in the mineral carbonation process of construction waste. Because the experimental conditions were low-injected CO_2 pressure and room temperature, the marl did not show an evident

transformation in its mineralogy. Another study carried out with a similar sample by Galán and Aparicio [35] showed that in the elapsed time at high temperature and pressure, the smectite, and later the illite, did not suffer any degradation.

The marl sample contains calcite ($CaCO_3$), quartz (SiO_2), illite ($(K,H_3O)(Al,Mg,Fe)_2(Si,Al)_4O_{10}[(OH)_2,(H_2O)]$), smectite ($(Ca,Na,H)(Al,Mg,Fe,Zn)_2(Si,Al)_4O_{10}(OH)_2$-$xH_2O$), mixed-layer illite-smectite, kaolinite ($Al_2Si_2O_5(OH)_4$), and a trace amount of dolomite ($CaMg(CO_3)_2$) and pyrite (FeS_2) (Figure 1). The semi-quantitative analysis of the minerals present in the original raw sample is shown in Table 1.

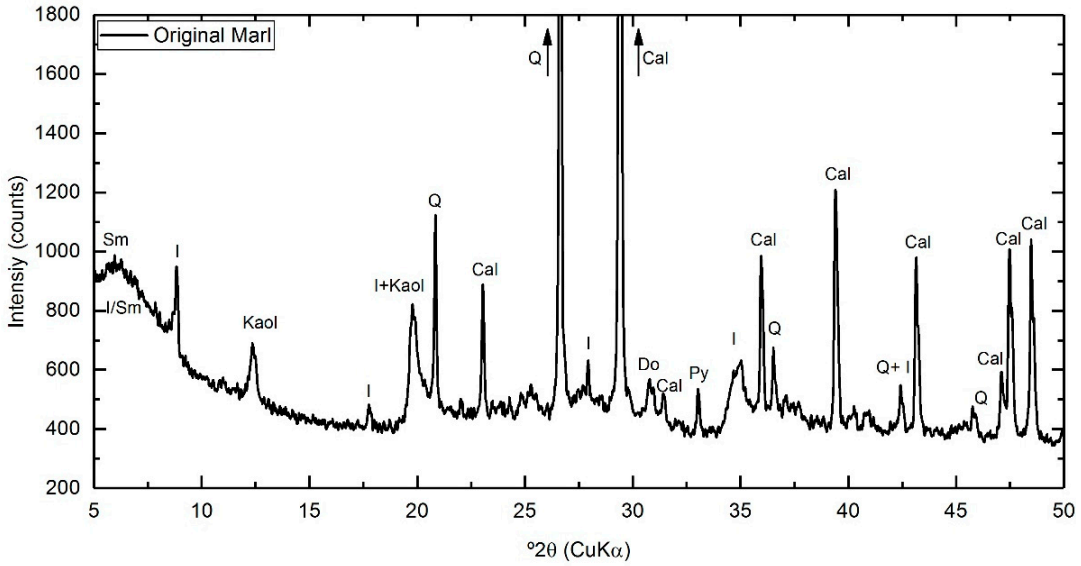

Figure 1. XRD-pattern of the raw blue marl. Cal: calcite; Q: quartz; Do: dolomite; I: illite; Kaol: kaolinite; Sm: smectite; I/Sm: mixed-layer illite-smectite.

Table 1. Mineralogical semi-quantification composition (wt%) of the original and treated samples after the reaction period of 120 and 240 h. σ: 3 x Estimated standard deviation = 99.7% repeatability limit, normal distribution; LOQ: limit of quantification, LOD: limit of detection, N.D.: not detected.

	Original				120 h				240 h			
Minerals	**wt%**	**±σ**	**LOQ**	**LOD**	**wt%**	**±σ**	**LOQ**	**LOD**	**wt%**	**±σ**	**LOQ**	**LOD**
Calcite	35.4	0.9	1.2	0.6	38.0	1.4	1.9	0.9	39.3	1.8	2.4	1.2
Dolomite	3.3	0.6	0.8	0.4	5.3	0.8	1.1	0.6	6.3	0.9	1.2	0.6
Quartz	14.0	0.5	0.6	0.3	11.8	0.6	0.8	0.4	11.5	0.6	0.8	0.4
Plagioclase (albite)	3.9	0.5	0.6	0.3	3.0	0.5	0.7	0.3	2.9	0.5	0.6	0.3
Pyrite	0.9	0.2	0.3	0.2	0.4	0.5	0.7	0.3	0.6	0.5	0.7	0.3
Siderite	N.D.	–	–	–	1.1	0.6	0.8	0.4	1.1	0.4	0.5	0.2
Illite	22.3	1.6	2.1	1.0	24.6	3.0	4.0	2.0	25.2	3.9	5.2	2.6
Kaolinite	5.2	0.8	1.1	0.6	5.4	0.8	1.1	0.6	6.0	1.0	1.3	0.7
Smectite	10.3	1.8	2.4	1.2	8.2	1.9	2.5	1.3	5.7	1.7	2.5	1.2
I/Sm	4.5	1.0	1.3	0.6	2.2	0.6	0.8	0.4	1.4	1.1	1.5	0.7

2.2. Methods and Characterization Procedures

The experiments were carried out in a steel reaction chamber, equipped with a pressure gauge and a thermocouple-controlled thermal heating jacket controlled by a thermocouple (Figure 2). The experimental suspensions were made by mixing 30 g of dry aggregates of different sizes of blue marl with 30 g of distilled deionized water (1:1 solid–water ratio). The pressure and temperature conditions required for the geological storage of supercritical CO_2 in deep formations must reach a pressure of 72 bar or more, with a temperature above 31 °C. CO_2, previously compressed in a pump to 100 bars to achieve the supercritical state,

was then injected and maintained at constant pressure. Experimental tests were carried out at 120 h and 240 h at 35 ° C, as was studied by Martin et al. in previous studies [33,34]. After the tests, the reaction chamber was depressurized by opening the gas outlet to allow CO_2 to slowly escape. The resulting sample was collected and dried at 70 °C for 24 h. Previously, the slurries were filtered using fiberglass filters (0.7-µm medium retention) and a vacuum pump. In this way, it was possible to separate a large part of the supernatant water from the solid sample.

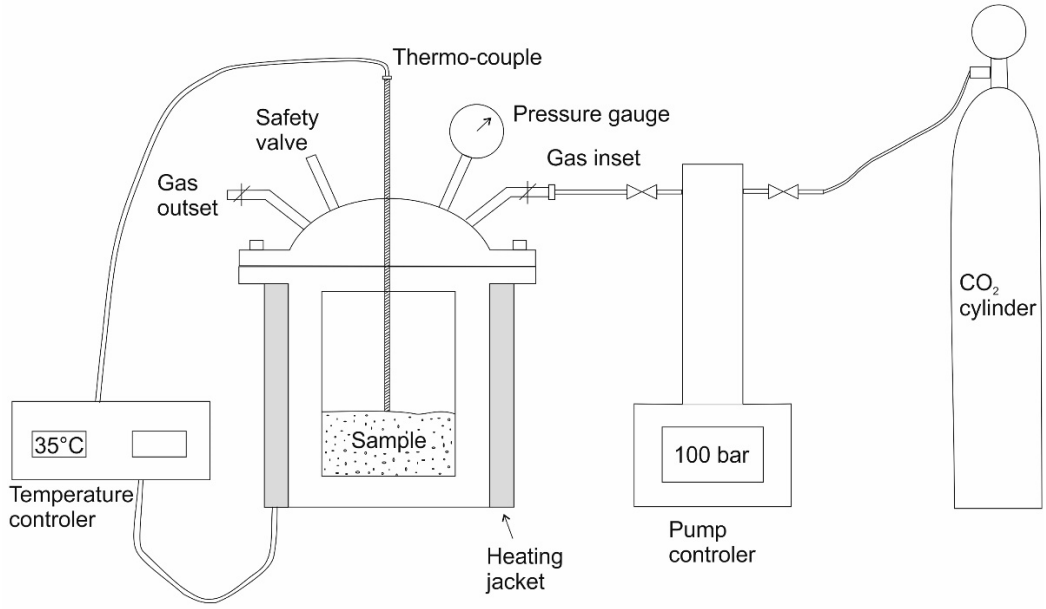

Figure 2. Schematic diagrams of the reaction vessel and auxiliary instruments (non-scaled).

The mineralogical composition of the dry treated sample was determined by X-ray diffraction analysis (XRD), using a Bruker D8 Advance diffractometer with standard monochromatic Cu-Kα radiation operating at 40 kV and 30 mA. Scanning was performed with a 0.015° 2θ step size, and at 0.1 s per step from 3° to 70°. Phyllosilicate identification was carried out on oriented specimens by clay fraction suspension. Three different states of the oriented samples were prepared: air dried (AD), saturated with ethylene glycol (EG), and heating at 550 °C. Oriented ADs were prepared when the suspension was dried at room temperature. EGs (Ethylene Glycol) were prepared by saturating air-dried oriented samples in ethylene glycol vapor in a desiccator at 60 °C for 24 h. The temperature treatments were set with air-dried oriented heated at 550 °C for 2 h. These types of preparation help characterize clay minerals with the swelling property of ethylene glycol solvation swelling, such as smectites, from those without this property, such as illite, and estimate the number of smectite layers in the mixed layer of illite-smectite. Heat treatment differentiated between clay minerals that collapse at temperatures below 550 °C and those that do not [36–39]. Additionally, Rietveld refinement was realized to determine the (semi)-quantitative composition of untreated and treated powdered samples. The software used for the refinement was Profex (version 3.14.0) [40].

Thermogravimetric analysis (TG) was performed in a TG Netzsch STA 409 PC. Samples (around 150 mg) were heated in an aluminum oxide crucible under a nitrogen atmosphere at 10 °C min^{-1} from room temperature to 1000 °C. Mass loss was measured by TG in the range of temperature 450–900 °C relative to total carbonated decomposition. The dihydroxylation of phyllosilicates in this range was considered.

Specific surface area (SSA-BET), micro- and nano-porosity were measured with an ASAP 2420 instrument (Micromeritics, Norcross, GA, USA) using adsorption of N_2 at liquid nitrogen temperature (−196 °C) and CO_2 at room temperature. Samples were outgassed for

180 min under vacuum at 150 °C to 10^{-3} Torr. The SSA was calculated using the classical Brunauer–Emmett–Teller theory (BET).

Inductively coupled plasma optical emission spectroscopy (ICP-OES), the Horiba Jobin Yvon ULTIMA 2 model instrument, was used to determine the amount of Al, Ca, Fe, K, Mg, Na, and Si in the reaction solutions of the supernatant obtained by separating the solid and liquid components by post-test filtration using fibreglass filters (0.7 µm medium retention) and a vacuum pump.

3. Results

To determine the transformation due to the interaction of $scCO_2$ with clay minerals in the sealing rock, the oriented aggregates prepared from the fine fraction were glycolate by solvation with ethylene glycol (EG) solvation and were subsequently examined by XRD (Figure 3). The composition of clay minerals and their evolution with $scCO_2$ tests and the labelling of the initial spacing positions d_{001} of smectite (Sm), illite (I), and kaolinite (Ka) (d_{001} ~ 17, 10 and 7.1 Å or 2θ ~ 5.1°, 8.8° and 12.4°, respectively), were included for better understanding. For illite and kaolinite, the X-ray patterns or intensity reflections were the same, with no significant variations. However, smectite and mixed-layer illite-smectite showed a decrease in intensity in the treated samples of the original.

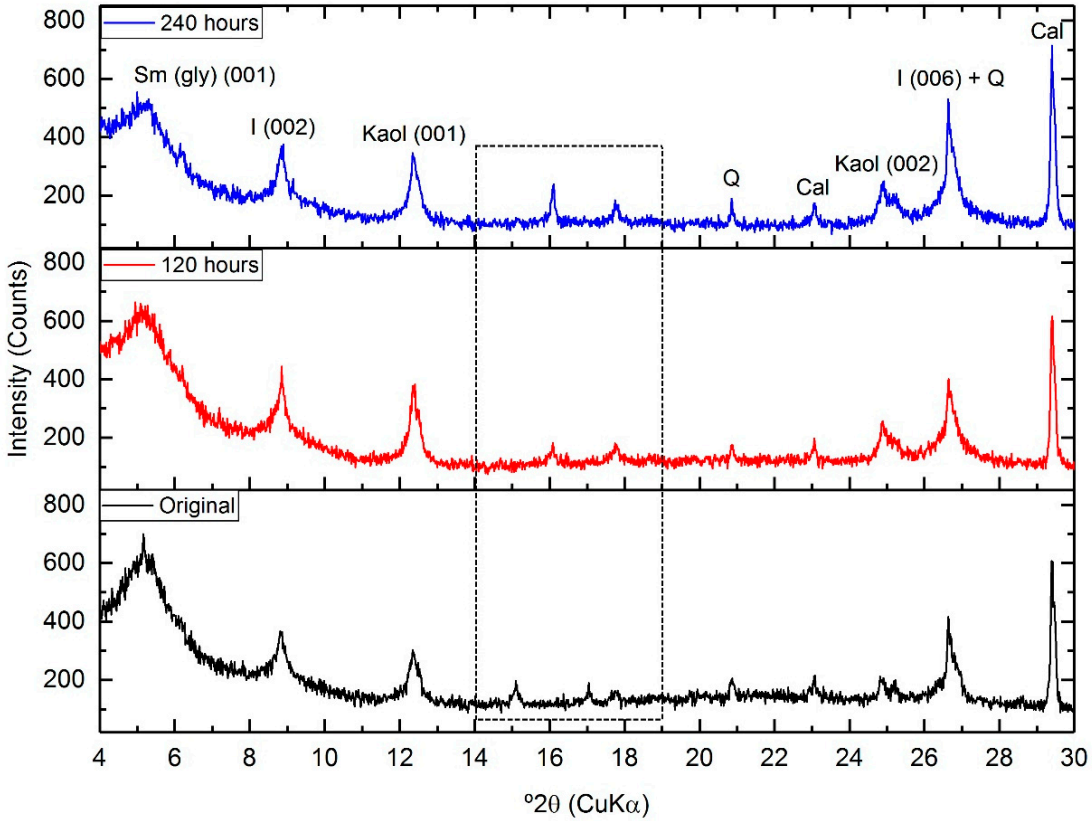

Figure 3. Comparison of XRD patterns of original blue marl oriented and original ethylene-glycol blue marl, after 120 and 240 h of interaction with sc-CO_2 (highlighted, see Figure 4).

In more detail (Figure 4), it was observed that after 120 h of reaction, the reflection d_{003} at 5.9 Å corresponding to the smectite practically collapsed. Likewise, the CO_2 interaction corresponds to the (70%) illite/(30%) smectite interstratified (002/003) with spacing close to 5.2 Å. The illitization reaction was also confirmed by a significant sharpening of the 5.0 Å peak ((004) illite). However, a new peak appears, identified as the reflection (002/003) of the interstratified illite/smectite with 40% illite [38,39]. In addition, a decrease in intensity and a shift in the low-angle peak corresponding to 001 of the smectite to lower spacing can

be observed. The shift of the gravity peak of glycol gravity-peak shift from 17.1 Å (5.15°2θ) to 16.5 Å (5.32°2θ), is more characteristic of a mixed-layer I/Sm (glycol) (Figure 3).

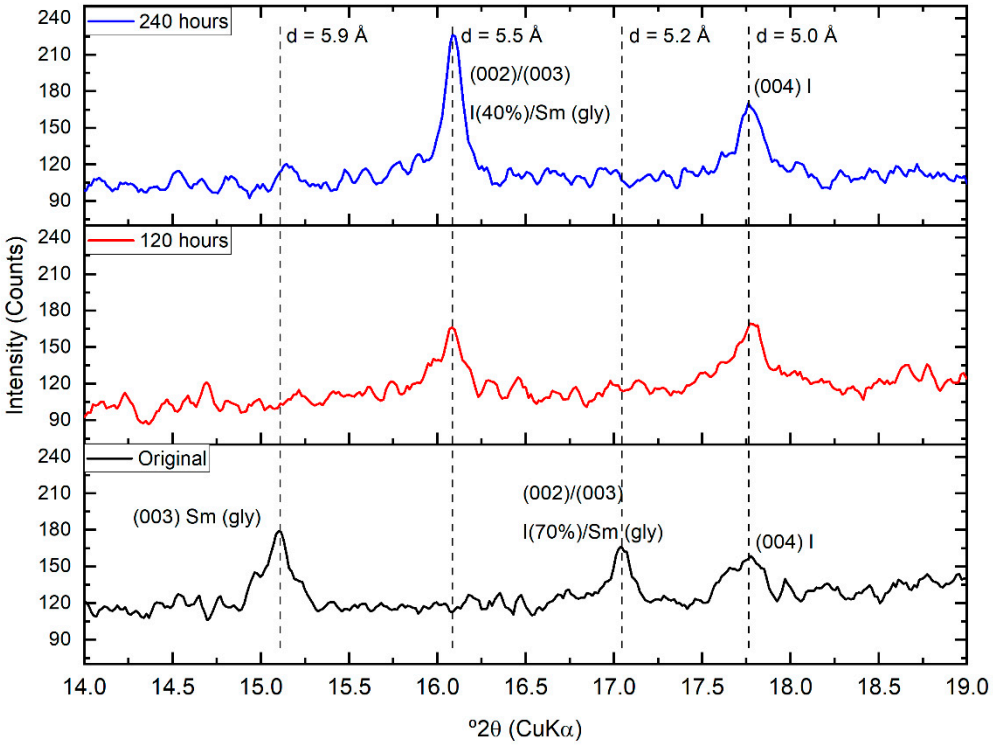

Figure 4. Comparison of XRD patterns (14–19° 2θ region) of the original blue marl and the original blue marl oriented and ethylene-glycol original blue marl, after 120 and 240 h of sc-CO_2 interaction.

At 240 h, a positive strengthening in the intensity of the reflection corresponding to the interstratified (40% illite) was observed, as well as a slight increase in intensity and a significant sharpening (higher symmetric peak) for the reflection of 004 of the illite (d_{004} ~ 5.0 Å). This slight increase in the intensity of the illite (Figure 3) was also observed for reflection 006 (d_{003} ~ 3.3 Å).

A possible dissolution and illitization process of the original smectite and mixed-layer was observed. The original mixed-layer with 70% illitic layers developed to 100% illitic layers (completed illitization) after 120 h. However, part of the original smectite began the illitization resulting in a new mixed layer (with around 40% illitic layers).

A (semi) quantitative analysis of the mineral phases present and their evolution with supercritical CO_2 treatments was performed by Rietveld refinement. Table 1 (Figures S1–S3 in the Supplementary Material) shows the (semi) quantitation results of the original (original blue marl) and treated common clay after 120 h and 240 h. A decrease in the smectite and interstratified content was observed, due to possible dissolution in acid medium (pH 3.3–3.5, estimated by Haghi et al. [41]). On the contrary, an increase in illite content was observed, along with an increase in carbonate mineral phases, calcite ($CaCO_3$), dolomite ($CaMg(CO_3)_2$), and siderite ($FeCO_3$); the siderite is not present in the original sample.

These results would agree with the fact that smectite in the treated samples was destroyed by dissolution, as well as the destruction or illitization of smectite in interstratified illite/smectite to illite. Additionally, a proportion of cations released in the dissolution/destruction of the mineral phases involved precipitate in the carbonate phases, chemically fixing CO_2. The precipitation of siderite (iron carbonate) was not significant. Iron cations (Fe^{3+}) must have come from dissolved phases in an acid medium, such as iron-rich smectites (nontronite or beidellite type), as well as from the pseudo-decomposition of illite layers in the interstratified.

The increase in carbonate phases was confirmed by the increase in weight loss observed by thermogravimetric analysis. In these tests, the original sample (untreated) had a weight loss in the temperature range 450–900 °C of 16.9 wt% compared to the samples treated at 120 h and 240 h with losses of 20.3 wt% and 21.7 wt%, respectively (Figure 5).

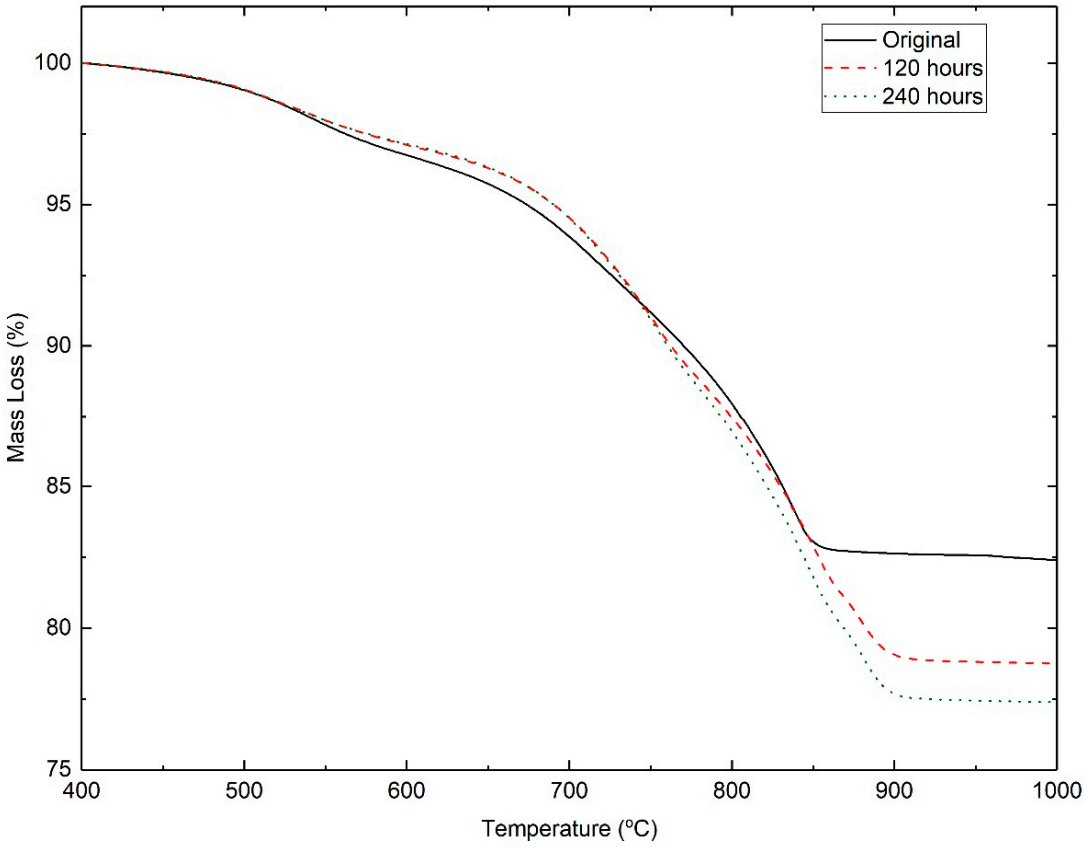

Figure 5. Thermogravimetric analysis of the original sample (solid line) and treated samples at 120 h (dash line) and 240 h (dotted line).

In general, the alteration mechanism takes place in two steps (Figure 6):

1. The mechanism of dissolution of smectite would be equivalent to that observed in other studies on the dissolution/alteration of swelling clay minerals (such as smectite and mixed-layers) by inorganic acid [42–47].
2. Leaching of Al, Mg, and Fe from the octahedral and tetrahedral sheets.

As a result, the process could result in illitization of the smectite structure into the illite structure, by loss of the exchangeable cations and modification of the octahedral layer.

On the other hand, in the studies described previously [42–47], different inorganic acids were introduced into the reaction as an activating agent of the swelling clay mineral activating agent; however, in the present study, the acid is carbonic acid. The initial reaction involved the dissolution of CO_2 in water to form carbonic acid, which dissociated to form $(HCO_3)^-$ and $(CO_3)^-$ ions.

The increase in Ca, Na, and Mg ions obtained by ICP-OES (Table 2) as a function of time with the original marl would be related to the exchange of interlayer cations from smectite to illite, as observed by the reduction of K (typical interlayer cation of illite). However, Ca also comes from a slight dissolution of the calcite in the marl.

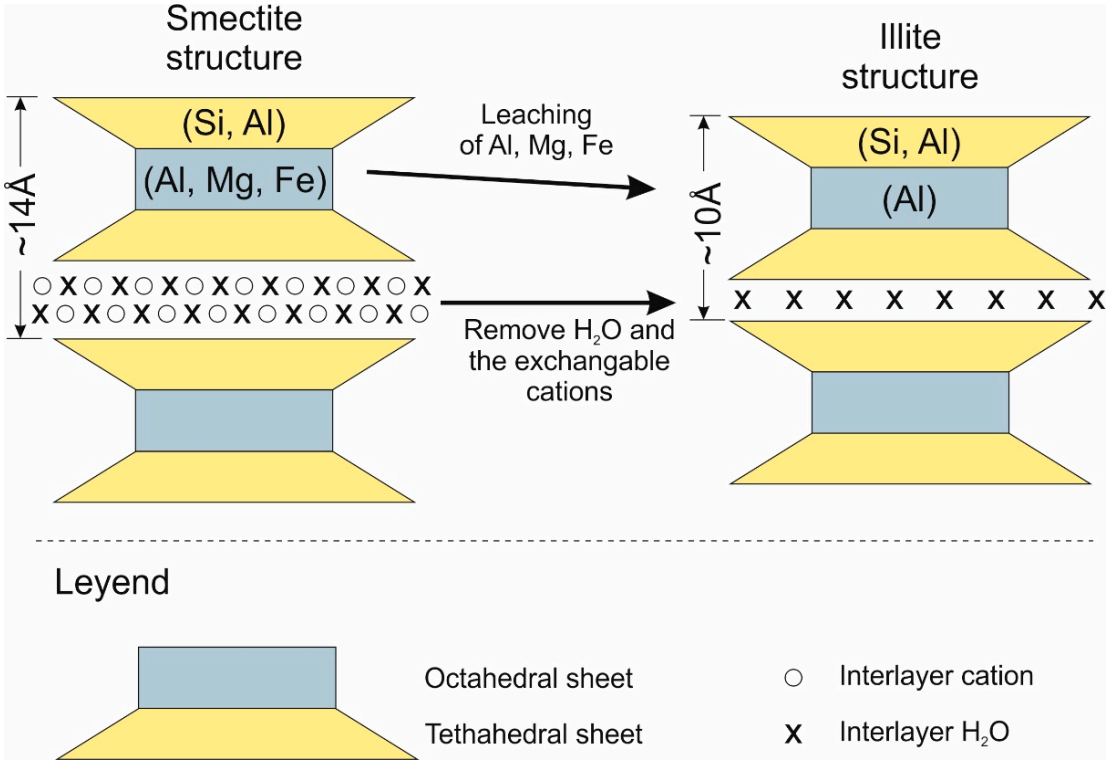

Figure 6. Schematic illustration of the proposed mechanisms for smectite illitization.

Table 2. Al, Ca, Fe, K, Mg, Na, and Si in the supernatant reaction solutions by ICP-EOS.

Element (mg/L)	Original	120 h	240 h
Al	<0.002	≤0.015	≤0.015
Ca	7.83 ± 0.16	46.1 ± 0.4	33.2 ± 0.9
Fe	0.004 ± 0.001	0.39 ± 0.07	0.67 ± 0.04
K	21.3 ± 0.9	10.1 ± 0.6	11.1 ± 0.6
Mg	21.1 ± 0.3	53.1 ± 0.5	72.1 ± 0.5
Na	19.2 ± 0.7	38.8 ± 0.5	41.5 ± 0.3
Si	2.50 ± 0.11	2.19 ± 0.09	3.46 ± 0.09

The leaching of the octahedral cations caused a relative increase in the Fe and Mg ion content in the reaction solutions. The results were non-conclusive for Al (below the quantification limit). However, authors previously referred to noted that leaching of the octahedral cations occurred in the order Mg, Fe, and Al [42,43,45,47].

After interaction with CO_2 or carbonic acid later, the specific surface area of BET (BET-SSA) and the pore volume increased (Table 3, and more details are in the Supplementary Materials file). After 120 h of reaction with CO_2, a significant increase in BET-SSA was observed, which maintained a slight increase over time until 240 h. The tendency of the pore volume also increased with time. On the other hand, the pore size decreases with the reaction time. Consequently, it appears that the marls in interaction with CO_2 undergo an increase in the specific surface area probably due to acid attack, increasing the pore volume, creating a new porosity of a lower average size than the pre-test porosity. The change in morphology could be caused by the modification of the smectite structure promoted by an acid attack. The reaction was primarily caused by the exchange of interlayer cations during the reaction and structural modification in the octahedral layer by the leaching of ions.

Table 3. Surface area, pore volume, and pore size by N_2-BET.

	BET Surface Area (m^2/g)	Pore Volume (cm^3/g)	Pore Size (nm)
Original	36.11	0.070	7.79
120 h	37.88	0.073	7.68
240 h	38.10	0.077	6.99

The N_2 adsorption-desorption isotherms of the pre- and post-test samples show identical patterns, with no significant change in the pore shape. However, the adsorbed amount of N_2 was slightly lower after 240 h of testing. This may be due to the reduction in pore size and the possible physical absorption of CO_2 in carbonation tests.

The specific surface area by CO_2, total pore volume, and total pore area increased directly with the reaction time, while the average pore area decreased again in size (smaller pore area) (Table 4). Both the N_2 and CO_2 adsorption tests seem to show an increase in porosity in the marls, which is smaller in all pore sizes than before the treatments.

Table 4. CO_2 adsorption summarized report.

		Original	120 h	240 h
BET Surface Area (m^2/g)		14.5298	15.1392	15.4480
Total Volume in Pores (cm^3/g)	≤1.066 nm	0.00233	0.00259	0.00287
Area in Pores (m^2/g)	>1.066 nm	8.953	8.769	8.787
Total Area in Pores (m^2/g)	≥0.367 nm	16.758	17.176	18.363

The adsorption of CO_2 isotherms showed a higher amount of adsorbed gas in treated samples, which was higher with a longer reaction time (Figure 7). This behavior could be related to the increase of smaller pore size (meso- to micro-pore).

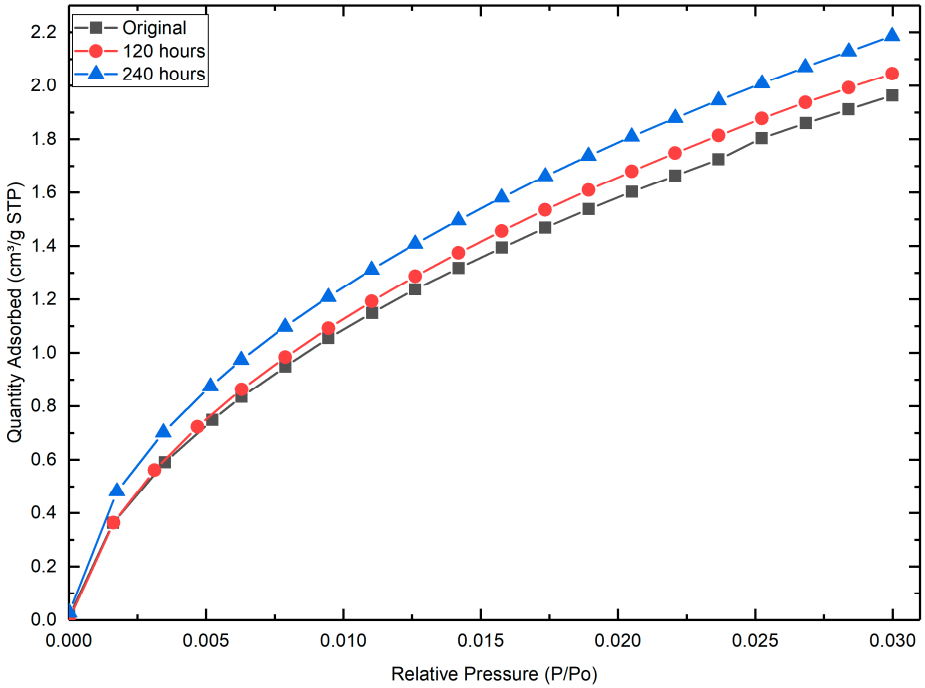

Figure 7. CO_2 adsorption isotherms of the pre- and post-test samples.

4. Discussion

For geological CO_2 storage (GCS), possible CO_2 leakage pathways impact three risk category areas: containment, site performance, and public perception [48]. Therefore, it

is important to understand the effects of mineralogical variability and heterogeneity on the geochemical response of the geological storage system to the injection of CO_2. The results of previous studies conclude that different mineralogical compositions significantly influence the patterns of geochemical and geophysical reactions, and hence the geological properties of CO_2 due to injection [14,49–51].

Since the main confining properties of the sealing rock are closely related to the content of the clayey material, it is crucial to understand the reactivity of these minerals in interaction with $scCO_2$ in wet conditions to assess the performance and safety of the geological storage system. Few studies have shown relevant experimental results and modelling models for illitization phenomena under CO_2 storage conditions for clay rocks [52,53]. This work explores these implications in common carbonate-rich clay such as marl, called blue marl, as well as assesses impacts on the sealing capacity of cap rock.

The first result of this study carried out under conditions close to those found in CO_2 geological storage systems, evidenced a process of illitization of smectite and mixed-layer illite–smectite that gradually transforms into illite under acidic conditions (carbonic acid). The illitization process of the smectite layers was observed by XRD.

The illitization process of the smectite layers was observed by XRD. The illitization process could be due to the dissolution/decomposition of the smectite layers that release Al^{3+}, Mg^{2+} and $Fe^{2+/3+}$ ions from the octahedral sheets, as shown by the ICP-EOS results. The decrease in the K content would be in opposition to the illite precipitation.

An important implication of the integrity of clayey seal rock caused by the illitization process of mixed-layer illite–smectite is the increase in porosity due to the alteration of the structures of the smectite layer [52,53], which is classically associated with a decrease in particle volume and loss of water molecules. Structurally, the smectite layers reduce their size in the basal direction, from 12–15 Å to the size of the illite (10 Å) by loss of hydration and change of exchange cations in the interlayer. A significant volume of illitization could result in the formation of microcracks that could interconnect over time and cause the undesirable leakage of gas from the confining region to materialize. CO_2 injected into a moist environment promotes the generation of carbonic acid and bicarbonate anions in solution, reducing the pH to between 3–5 [22,25,54]. Reduced pH causes the weathering of aluminosilicates in the rock, such as smectites. It also causes the dissolution of carbonate minerals, such as calcite in the marl studied.

The dissolution of primary minerals and the consequent contribution of cations ($Fe^{2+/3+}$, Ca^{2+}, Mg^{2+}, Na^{+}, and Al^{3+}) buffer the pH and can achieve alkaline solution values (around 7–8) [24]. These free cations, combined with carbonic anions, precipitate in secondary carbonate minerals, mainly Ca^{2+}, Mg^{2+} and/or Fe^{2+} (+4 wt% calcite, +3 wt% dolomite and +1 wt% siderite, Table 1), chemically fixing a proportion of CO_2 [10,14,24–26].

On the one hand, the dissolution of the primary minerals of the rock would increase porosity. However, secondary precipitation of carbonates would cause a reduction in porosity [10,22,24,26,55]. Aljamann et al. [56] showed that an increase in illite content in shale formations was related to an increase in surface area and pore capacity, allowing additional space for CO_2 absorption. From a sealing efficiency point of view, an increase in porosity will weaken the sealing capacity of the capped rock, while a decrease in porosity will improve the sealing capacity of a geological storage site [57].

Finally, it should be considered that clayey rocks have a heterogeneous distribution of constituent minerals, as well as the presence of veins. Carbonate and dissolution-susceptible mineral veins of considerable volume may be a potential risk for failure and leakage of stored gas.

5. Conclusions

Changes in smectite and mixed-layer illite/smectite minerals from clayey rocks used as cap rock were studied under geological CO_2 storage.

The high CO_2 pressure used in geological storage induces irreversible changes in the structure of clay mineral particles in the clayey cap rock. Under carbonic acid conditions,

promoted by the dissolution of CO_2 in water, a combined dissolution and illitization of smectite was confirmed by changes in exchangeable cations determined by ICP-EOS (from 21.3 to 11.1 mg/L for K, typical in illite). Additionally, a proportion of cations released in the dissolution/destruction of the involved mineral phases precipitate in the carbonate phases, calcite, dolomite and siderite, chemically fixing CO_2. Acidic solutions had a significant impact on both the dissolution of mixed-layer illite—smectite and carbonate minerals and the precipitation of secondary minerals.

The multipoint BET technique was used to obtain geometrical properties of the pores, such as the specific surface area (from 36.1 to 38.1 m^2/g by N_2 and from 14.5 to 15.4 m^2/g by CO_2 adsorption test) and the pore volume (slightly decrease from 0.070 to 0.077 cm^3/g), which were affected by mineral dissolution and precipitation. These changes were indicative that CO_2 interaction can affect rock reactivity over a long storage time.

Slight porosity in changes (from 7.8 to 7.0 nm, pore size) are related to the alteration, dissolution, and secondary precipitation of the constituent minerals in the clay-sealing rock. Together with the possible heterogeneity of the mineral composition of the cap rock, the integrity of the cap rock is risked due to the massive dissolution of minerals, encouraging the interconnection of undesirable leakage pathways of the stored CO_2.

Therefore, knowledge of the interaction between CO_2 and sealing rock and its implications for GCS requires extensive studies to ensure long-term safety.

Supplementary Materials: The following supporting information can be downloaded at: https://www.mdpi.com/article/10.3390/app122211477/s1, Figure S1: Rietveld analysis pattern of the powder diffraction data of Original Marl; Figure S2: Rietveld analysis pattern of the powder diffraction data of the marl tested during 120 h; Figure S3: Rietveld analysis pattern of marl powder diffraction data tested during 240 h; Figure S4: Surface area, pore volume, and pore size by N_2-BET; Figure S5: N_2 adsorption-desorption isotherms of the pre- and post-test samples; Figure S6: BET-surface area, total volume in pores, area, and total in pores by CO_2 adsorption tests; Figure S7: CO_2 adsorption isotherms of the pre- and post-test samples.

Author Contributions: Conceptualization, D.M. and P.A.; methodology, D.M.; formal analysis, D.M., P.A., S.G. and M.M.M.-V.; writing—original draft preparation, D.M. and P.A.; writing—review and editing, D.M., P.A., S.G. and M.M.M.-V.; supervision, S.G. and M.M.M.-V. All authors have read and agreed to the published version of the manuscript.

Funding: This research was funded by the Junta de Andalucía (Conserjería de Economía y Conocimiento) grand number [P12-RNM-568 MO project] and the contract of Domingo Martín granted by the V Plan Propio de Investigación de la Universidad de Sevilla.

Institutional Review Board Statement: Not applicable.

Informed Consent Statement: Not applicable.

Data Availability Statement: Not applicable.

Acknowledgments: I XRD: BET, and ICP-EOS analyses were performed using the facilities of the General Research Center of the University of Seville (CITIUS). Domingo Martín acknowledges Mercedes Maroto-Valer, Susana García and the Research Centre for Carbon Solutions (RCCS) group for facilitating my short research stay with them.

Conflicts of Interest: The authors declare no conflict of interest.

References

1. Nityashree, N.; Price, C.A.H.; Pastor-Perez, L.; Manohara, G.V.; Garcia, S.; Maroto-Valer, M.M.; Reina, T.R. Carbon stabilised saponite supported transition metal-alloy catalysts for chemical CO_2 utilisation via reverse water-gas shift reaction. *Appl. Catal. B Environ.* **2020**, *261*, 118241. [CrossRef]
2. Rogelj, J.; Geden, O.; Cowie, A.; Reisinger, A. Three ways to improve net-zero emissions targets. *Nature* **2021**, *591*, 365–368. [CrossRef] [PubMed]
3. Rogelj, J.; Schaeffer, M.; Meinshausen, M.; Knutti, R.; Alcamo, J.; Riahi, K.; Hare, W. Zero emission targets as long-term global goals for climate protection. *Environ. Res. Lett.* **2015**, *10*, 105007. [CrossRef]

4. United Nations Summary of the Paris Agreement. In *Adoption of the Paris Agreement*; United Nations Framework Convention on Climate Change (UNFCCC): Paris, France, 2015.
5. Gabrielli, P.; Gazzani, M.; Mazzotti, M. The Role of Carbon Capture and Utilization, Carbon Capture and Storage, and Biomass to Enable a Net-Zero-CO_2 Emissions Chemical Industry. *Ind. Eng. Chem. Res.* **2020**, *59*, 7033–7045. [CrossRef]
6. Becattini, V.; Gabrielli, P.; Mazzotti, M. Role of carbon capture, storage, and utilization to enable a Net-Zero-CO_2-emissions aviation sector. *Ind. Eng. Chem. Res.* **2021**, *60*, 6848–6862. [CrossRef]
7. Ajoma, E.; Saira; Sungkachart, T.; Ge, J.; Le-Hussain, F. Water-saturated CO_2 injection to improve oil recovery and CO_2 storage. *Appl. Energy* **2020**, *266*, 114853. [CrossRef]
8. Metz, B.; Davidson, O.; De Coninck, H.; Loos, M.; Meyer, L.; IPCC. *IPCC Special Report on Carbon Dioxide Capture and Storage*; Working Group III; Intergovernmental Panel on Climate Change: Geneva, Switzerland, 2005; Volume 2, ISBN 9780521866439.
9. Busch, A.; Amann, A.; Bertier, P.; Waschbusch, M.; Krooss, B.M. The significance of caprock sealing integrity for CO_2 storage. In Proceedings of the SPE International Conference on CO_2 Capture, Storage and Utilization, New Orleans, LA, USA, 10–12 November 2010; pp. 300–307.
10. Fatah, A.; Bennour, Z.; Ben Mahmud, H.; Gholami, R.; Hossain, M.M. A review on the influence of CO_2/shale interaction on shale properties: Implications of CCS in shales. *Energies* **2020**, *13*, 3200. [CrossRef]
11. Harvey, O.R.; Qafoku, N.P.; Cantrell, K.J.; Lee, G.; Amonette, J.E.; Brown, C.F. Geochemical implications of gas leakage associated with geologic CO_2 storage—A qualitative review. *Environ. Sci. Technol.* **2013**, *47*, 23–36. [CrossRef]
12. Olabode, A.; Radonjic, M. Shale Caprock/Acidic Brine Interaction in Underground CO_2 Storage. *J. Energy Resour. Technol.* **2014**, *136*, 1–6. [CrossRef]
13. Scherer, G.W.; Celia, M.A.; Prevost, J.H.; Bachu, S.; Bruant, R.G.; Duguid, A.; Fuller, R.; Gasda, S.E.; Radonjic, M.; Vicjit-Vadakna, W. Leakage of CO_2 through abandoned wells: Role of corrosion of cement. In *The CO_2 Capture and Storage Project (CCP) for Carbon Dioxide Storage in Deep Geologic Formations for Climate Change Mitigation*; Benson, S.M., Ed.; Elsevier: London, UK, 2004; pp. 827–848.
14. Tian, H.; Xu, T.; Zhu, H.; Yang, C.; Ding, F. Heterogeneity in mineral composition and its impact on the sealing capacity of caprock for a CO_2 geological storage site. *Comput. Geosci.* **2019**, *125*, 30–42. [CrossRef]
15. Zhang, M.; Bachu, S. Review of integrity of existing wells in relation to CO_2 geological storage: What do we know? *Int. J. Greenh. Gas Control* **2011**, *5*, 826–840. [CrossRef]
16. Jia, B.; Chen, Z.; Xian, C. Investigations of CO_2 storage capacity and flow behavior in shale formation. *J. Pet. Sci. Eng.* **2022**, *208*, 109659. [CrossRef]
17. Gaus, I. Role and impact of CO_2-rock interactions during CO_2 storage in sedimentary rocks. *Int. J. Greenh. Gas Control* **2010**, *4*, 73–89. [CrossRef]
18. Seifritz, W. CO_2 disposal by means of silicates. *Nature* **1990**, *345*, 486. [CrossRef]
19. Johnson, J.W.; Nitao, J.J.; Knauss, K.G. Reactive transport modelling of CO_2 storage in saline aquifers to elucidate fundamental processes, trapping mechanisms and sequestration partitioning. *Geol. Soc. Spec. Publ.* **2004**, *233*, 107–128. [CrossRef]
20. Huijgen, W.J.J.; Comans, R.N.J. *Carbon Dioxide Sequestration by Mineral Carbonation. Literature Review*; Report from the Energy research Centre of the Netherlands; Energy research Centre of the Netherlands: Pettern, The Netherlands, 2003.
21. Teir, S.; Revitzer, H.; Eloneva, S.; Fogelholm, C.-J.; Zevenhoven, R. Dissolution of natural serpentinite in mineral and organic acids. *Int. J. Miner. Process.* **2007**, *83*, 36–46. [CrossRef]
22. Espinoza, D.N.; Santamarina, J.C. CO_2 breakthrough—Caprock sealing efficiency and integrity for carbon geological storage. *Int. J. Greenh. Gas Control* **2017**, *66*, 218–229. [CrossRef]
23. Gaus, I.; Azaroual, M.; Czernichowski-Lauriol, I. Reactive transport modelling of the impact of CO_2 injection on the clayey cap rock at Sleipner (North Sea). *Chem. Geol.* **2005**, *217*, 319–337. [CrossRef]
24. Hemme, C.; van Berk, W. Change in cap rock porosity triggered by pressure and temperature dependent CO_2–water–rock interactions in CO_2 storage systems. *Petroleum* **2017**, *3*, 96–108. [CrossRef]
25. Tian, H.; Xu, T.; Li, Y.; Yang, Z.; Wang, F. Evolution of sealing efficiency for CO_2 geological storage due to mineral alteration within a hydrogeologically heterogeneous caprock. *Appl. Geochem.* **2015**, *63*, 380–397. [CrossRef]
26. Tian, H.; Pan, F.; Xu, T.; McPherson, B.J.; Yue, G.; Mandalaparty, P. Impacts of hydrological heterogeneities on caprock mineral alteration and containment of CO_2 in geological storage sites. *Int. J. Greenh. Gas Control* **2014**, *24*, 30–42. [CrossRef]
27. Jia, B.; Xian, C.G. Permeability measurement of the fracture-matrix system with 3D embedded discrete fracture model. *Pet. Sci.* **2022**, *19*, 1757–1765. [CrossRef]
28. Little, M.G.; Jackson, R.B. Potential impacts of leakage from deep CO_2 geosequestration on overlying freshwater aquifers. *Environ. Sci. Technol.* **2010**, *44*, 9225–9232. [CrossRef] [PubMed]
29. Lu, J.; Partin, J.W.; Hovorka, S.D.; Wong, C. Potential risks to freshwater resources as a result of leakage from CO_2 geological storage: A batch-reaction experiment. *Environ. Earth Sci.* **2010**, *60*, 335–348. [CrossRef]
30. Lyu, Q.; Tan, J.; Li, L.; Ju, Y.; Busch, A.; Wood, D.A.; Ranjith, P.G.; Middleton, R.; Shu, B.; Hu, C.; et al. The role of supercritical carbon dioxide for recovery of shale gas and sequestration in gas shale reservoirs. *Energy Environ. Sci.* **2021**, *14*, 4203–4227. [CrossRef]
31. Wang, H.; Li, G.; Shen, Z. A feasibility analysis on shale gas exploitation with supercritical carbon dioxide. *Energy Sources Part A Recover. Util. Environ. Eff.* **2012**, *34*, 1426–1435. [CrossRef]

32. Middleton, R.S.; Carey, J.W.; Currier, R.P.; Hyman, J.D.; Kang, Q.; Karra, S.; Jiménez-Martínez, J.; Porter, M.L.; Viswanathan, H.S. Shale gas and non-aqueous fracturing fluids: Opportunities and challenges for supercritical CO_2. *Appl. Energy* **2015**, *147*, 500–509. [CrossRef]
33. Martín, D.; Aparicio, P.; Galán, E. Mineral carbonation of ceramic brick at low pressure and room temperature. A simulation study for a superficial CO_2 store using a common clay as sealing material. *Appl. Clay Sci.* **2018**, *161*. [CrossRef]
34. Martín, D.; Aparicio, P.; Galán, E. Time evolution of the mineral carbonation of ceramic bricks in a simulated pilot plant using a common clay as sealing material at superficial conditions. *Appl. Clay Sci.* **2019**, *180*, 5191. [CrossRef]
35. Galán, E.; Aparicio, P. Experimental study on the role of clays as sealing materials in the geological storage of carbon dioxide. *Appl. Clay Sci.* **2014**, *87*, 22–27. [CrossRef]
36. Bradley, W.F. Molecular associations between montmorillonite and some polyfunctional organic liquids1. *J. Am. Chem. Soc.* **1945**, *67*, 975–981. [CrossRef]
37. Brindley, G.W.; Brown, G. *Crystal Structures of Clay Minerals and Their X-ray Identification*, 1st ed.; The Mineralogical Society of Great Britain and Ireland: London, UK, 1980; Volume 5, ISBN 0903056089.
38. Moore, D.M.; Reynolds Jr, R.C. *X-ray Diffraction and the Identification and Analysis of Clay Minerals*, 2nd ed.; Oxford University Press (OUP): New York, NY, USA, 1997; ISBN 019505170X.
39. Środoń, J. Identification and Quantitative Analysis of Clay Minerals. In *Handbook of Clay Science*; Elsevier: Amsterdam, The Netherland, 2013; Volume 5, pp. 25–49, ISBN 9780080982595.
40. Doebelin, N.; Kleeberg, R. Profex: A graphical user interface for the Rietveld refinement program BGMN. *J. Appl. Crystallogr.* **2015**, *48*, 1573–1580. [CrossRef] [PubMed]
41. Haghi, R.K.; Chapoy, A.; Peirera, L.M.C.; Yang, J.; Tohidi, B. pH of CO_2 saturated water and CO_2 saturated brines: Experimental measurements and modelling. *Int. J. Greenh. Gas Control* **2017**, *66*, 190–203. [CrossRef]
42. Jeon, P.R.; Kim, D.W.; Lee, C.H. Dissolution and reaction in a CO_2-brine-clay mineral particle system under geological CO_2 sequestration from subcritical to supercritical conditions. *Chem. Eng. J.* **2018**, *347*, 1–11. [CrossRef]
43. Komadel, P. Acid activated clays: Materials in continuous demand. *Appl. Clay Sci.* **2016**, *131*, 84–99. [CrossRef]
44. Ni, X.; Li, Q.; Chen, W. Dissolution kinetics of Si and Al from montmorillonite in carbonic acid solution. *Int. J. Coal Sci. Technol.* **2014**, *1*, 31–38. [CrossRef]
45. Pentrák, M.; Madejová, J.; Komadel, P. Effect of chemical composition and swelling on acid dissolution of 2: 1 clay minerals. *Philos. Mag.* **2010**, *90*, 2387–2397. [CrossRef]
46. Dri, M.; Sanna, A.; Maroto-Valer, M.M. Mineral carbonation from metal wastes: Effect of solid to liquid ratio on the efficiency and characterization of carbonated products. *Appl. Energy* **2014**, *113*, 515–532. [CrossRef]
47. Steudel, A.; Batenburg, L.F.; Fischer, H.R.; Weidler, P.G.; Emmerich, K. Alteration of swelling clay minerals by acid activation. *Appl. Clay Sci.* **2009**, *44*, 105–115. [CrossRef]
48. Pawar, R.J.; Bromhal, G.S.; Carey, J.W.; Foxall, W.; Korre, A.; Ringrose, P.S.; Tucker, O.; Watson, M.N.; White, J.A. Recent advances in risk assessment and risk management of geologic CO_2 storage. *Int. J. Greenh. Gas Control* **2015**, *40*, 292–311. [CrossRef]
49. Glassley, W.E.; Simmons, A.M.; Kercher, J.R. Mineralogical heterogeneity in fractured, porous media and its representation in reactive transport models. *Appl. Geochem.* **2002**, *17*, 699–708. [CrossRef]
50. Lai, P.; Moulton, K.; Krevor, S. Pore-scale heterogeneity in the mineral distribution and reactive surface area of porous rocks. *Chem. Geol.* **2015**, *411*, 260–273. [CrossRef]
51. Zhao, Y.; Zhang, Y.; Liu, J.; Gao, J.; Ji, Z.; Guo, X.; Liu, J.; Yuan, J. Trash to treasure: Seawater pretreatment by CO_2 mineral carbonation using brine pretreatment waste of soda ash plant as alkali source. *Desalination* **2017**, *407*, 85–92. [CrossRef]
52. Kohler, E.; Parra, T.; Vidal, O. Clayey cap-rock behavior in H_2O-CO_2 media at low pressure and temperature conditions: An experimental approach. *Clays Clay Miner.* **2009**, *57*, 616–637. [CrossRef]
53. Credoz, A.; Bildstein, O.; Jullien, M.; Raynal, J.; Trotignon, L.; Pokrovsky, O. Mixed-layer illite-smectite reactivity in acidified solutions: Implications for clayey caprock stability in CO_2 geological storage. *Appl. Clay Sci.* **2011**, *53*, 402–408. [CrossRef]
54. Liu, F.; Lu, P.; Zhu, C.; Xiao, Y. Coupled reactive flow and transport modeling of CO_2 sequestration in the Mt. Simon sandstone formation, Midwest U.S.A. *Int. J. Greenh. Gas Control* **2011**, *5*, 294–307. [CrossRef]
55. Pearce, J.K.; Dawson, G.K.W.; Law, A.C.K.; Biddle, D.; Golding, S.D. Reactivity of micas and cap-rock in wet supercritical CO_2 with SO_2 and O_2 at CO_2 storage conditions. *Appl. Geochem.* **2016**, *72*, 59–76. [CrossRef]
56. Aljamaan, H.; Holmes, R.; Vishal, V.; Haghpanah, R.; Wilcox, J.; Kovscek, A.R. CO_2 Storage and Flow Capacity Measurements on Idealized Shales from Dynamic Breakthrough Experiments. *Energy Fuels* **2017**, *31*, 1193–1207. [CrossRef]
57. Rani, S.; Padmanabhan, E.; Bakshi, T.; Prusty, B.K.; Pal, S.K. CO_2 sorption and rate characteristics in micropores of shales. *J. Nat. Gas Sci. Eng.* **2019**, *68*, 102903. [CrossRef]